ChemElectroChem

Research Article
doi.org/10.1002/celc.202500337

Chemistry Europe
European Chemical Societies Publishing

www.chemelectrochem.org

Valorization of Glycerol Through 2,2,6,6-Tetramethyl-1-Piperidine-N-Oxyl (TEMPO)-Catalyzed Electrochemical Oxidation with High C3 Product Selectivity: Impact of Stirred Bulk Versus Flow Electrolysis

Yuanya Zhao, Rachel N. Gaines, Adolfo I. B. Romo, Juan A. Rojas, Paul J. A. Kenis, and Joaquín Rodríguez-López*

Conversion of glycerol to value-added products is an attractive solution to the oversupply of this byproduct of biofuel production. The glycerol oxidation reaction (GOR) may form product mixtures derived from the scission of the three-carbon (C3) glycerol backbone, generating one- (C1) or two-carbon (C2) species. Here, the bulk and flow electrolysis (FE) of the 2,2,6,6-tetramethyl-1-piperidine-N-oxyl (TEMPO)-mediated GOR reaction is explored to produce a valorized C3 product, highlighting key selectivity differences between the two methods despite using the same optimized electrolyte composition. Increasing the pH of the solution dramatically increases GOR activity but presents a tradeoff with the stability of TEMPO. At an optimal pH of 10.6 in carbonate buffer in a batch reactor, the reaction proceeds with higher than 90% yield via a 10-electron oxidation to mesoxalic acid, a C3 product. FE at much lower Reynolds number yields significantly lower selectivity toward C3, demonstrating a high sensitivity to mass transport. The work sheds light on the opportunities toward selectively producing C3 products from GOR as well as the importance of mass transfer considerations for the valorization of this key bio-feedstock and for others involving mediated electrocatalysis.

1. Introduction

The increasing wide employment of biofuel over the past few decades has helped global decarbonization efforts.[1,2] However, a new issue has been imposed on the environment by the biofuel industry: the glut of glycerol. Glycerol is one of the major by-products generated during the production of both biodiesel and bioethanol,[3–5] but its decoupled production and demand is causing significant waste and pollution worldwide.[6] The annual global biodiesel production in 2024 was about 69 million tons,[5] producing on the order of 7 million tons of crude glycerol (10% by weight of biodiesel produced; still significant fractions of methanol, water, base, and ash), which contains about 5 million tons of glycerol. This amount significantly exceeds the global market demand for glycerol, which is also produced by synthesis from propylene.

Y. Zhao, A. I. B. Romo, J. A. Rojas, J. Rodríguez-López
Department of Chemistry
University of Illinois Urbana–Champaign
600 South Mathews Avenue, Urbana, IL 61801, USA
E-mail: joaquinr@illinois.edu

R. N. Gaines, J. A. Rojas, P. J. A. Kenis
Department of Chemical and Biomolecular Engineering
University of Illinois Urbana–Champaign
600 South Mathews Avenue, Urbana 61801, IL, USA

This surplus has called for the development of economically feasible processes to utilize the underpriced glycerol resource. Glycerol valorization, i.e., chemically converting it to high-value products, is the most attractive approach because it is less dependent on fluctuations of the glycerol market price and can achieve a higher profit margin.[6] Intensive research efforts have been devoted to studying glycerol valorization through a variety of pathways, including glycerol reforming,[7–9] biocatalytic fermentation,[9–11] hydrogenolysis,[12–14] dehydration,[15–17] polymerization,[15] and oxidation.[18–20] Among all approaches, glycerol oxidation is one of the most promising routes to obtain valorized products such as dihydroxyacetone (DHA), glyceric acid (GLA), tartronic acid (TA), mesoxalic acid (MA), glyceraldehyde (GLAD), glycolic acid (GA), and formic acid (FA). These products have a wide range of applications in chemistry research, pharmaceuticals, cosmetics, and agriculture. Their structures, shown in **Scheme1**A, range from those containing one or two carbon atoms (i.e., C1–C2, resulting from scission of the C—C bond in glycerol) to those preserving the original three-carbon backbone of glycerol (C3).

More specifically, electrochemical conversion of glycerol via the glycerol oxidation reaction (GOR) has shown its superiority over traditional chemical oxidation and raised great interest due to its environmentally-friendliness and high conversion efficiency.[21–27] The feasibility and profitability of GOR are highly dependent on the activity and selectivity of the electrocatalysts. Most studies on GOR electrocatalysts have been focused on noble metals such as Pt, Pd, and Au, which

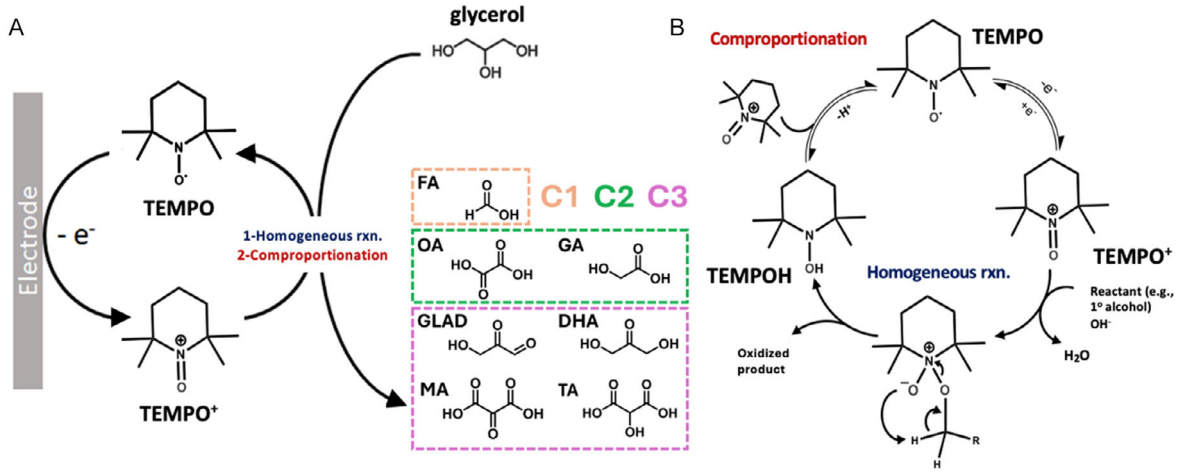

Scheme 1. Schematic of the mechanism of TEMPO-catalyzed GOR. A) Simplified depiction of the electrocatalytic cycle involving the oxidation of glycerol by electrogenerated 2,2,6,6-tetramethyl-1-piperidine-N-oxyl ($TEMPO^+$) to generate C1, C2, and C3 products. FA = formic acid, OA = oxalic acid, GA = glycolic acid, GLAD = glyceraldehyde, DHA = dihydroxyacetone, TA = tartronic acid, and MA = mesoxalic acid. B) Detailed mechanism of alcohol oxidation catalyzed by TEMPO including the homogeneous reaction and comproportionation steps summarized in part A.

generally suffer from the drawbacks of high cost and their susceptibility to being poisoned by by-products such as CO.[4] In addition, these materials often lead to complex product mixtures as they produce mixtures of C1-C3 molecules, with selectivity values highly dependent on the material and reaction conditions.

In this article, we propose to use 2,2,6,6-tetramethyl-1-piperidine-N-oxyl (TEMPO) radicals as a homogeneous molecular electrocatalyst for GOR, as shown in Scheme 1A. TEMPO can selectively catalyze the oxidation of a wide range of alcohols and aldehydes at room temperature and under mild aqueous conditions,[28] and our group has used it both as a practical electrocatalytic mediator for bulk electrolysis (BE) of high concentrations of alcohols (e.g., selective 0.5 M isopropanol to acetone)[29] and as a model electrocatalyst for the exploration of automated electrocatalysis platforms.[30,31] Due to its structural and synthetic simplicity, high activity, and versatility, TEMPO is considered one of the most promising alternatives to noble metal catalysts. As a result, it has found widespread applications as an important catalyst for alcohol oxidation in both industrial manufacturing and laboratory research.[32] Scheme 1B provides a more detailed view of the electrocatalytic mechanism for the oxidation of glycerol with TEMPO. An initial electrochemical oxidation step in which the electrode withdraws an electron from TEMPO, converts the radical to a catalytically active oxoammonium salt, $TEMPO^+$. Then, $TEMPO^+$ oxidizes the alcohol substrate in a pH-dependent process into corresponding aldehydes, ketones, or carboxylic acids and turns the mediator into a hydroxylamine, TEMPOH. Lastly, a comproportionation step involving the oxidation of TEMPOH by $TEMPO^+$ in the diffusion layer leads to the regeneration of two molecules of TEMPO radical, forming a complete catalytic cycle.[28,29] The voltammetric current-potential response during this cycle depends strongly on the shape and current intensity on variables such as the scan rate, the concentration of alcohol, the concentration of TEMPO, pH, and the rate constant for the homogeneous reaction.[31]

Prior work has given insight into TEMPO's potential for the electrocatalytic GOR.[33,34] TEMPO has also been used in combination with an enzyme and oxalate oxidase, forming a hybrid electrocatalytic cascade, for the complete oxidation of glycerol.[35] Ciriminna et al. reported a one-pot chemical method for the oxidation of glycerol to MA mediated by TEMPO and cocatalyzed by Br^-.[36] These previous experimental results highlight TEMPO's ability to specifically target the oxidation of glycerol while circumventing C—C bond cleavage, unlike other metallic catalysts. However, investigations into how free TEMPO in an electrocatalytic medium may interact with different electrolysis architectures, e.g., batch BE versus flow, its ability to oxidize high concentrations of glycerol, and its robustness in producing C3 products are scarce in the literature.[23]

Here, we present a detailed investigation on the activity, stability, and product selectivity of TEMPO for GOR through cyclic voltammetry (CV), BE, and flow electrolysis (FE) experiments, including rigorous product identification and quantification with high-performance liquid chromatography (HPLC). We show that the pH of the electrolyte solution has a strong impact on TEMPO's activity and stability. After identifying the ideal conditions for maximum catalytic performance, we compare the performance of the TEMPO-catalyzed GOR system in BE conditions to a FE setup with the intention of getting closer to the conditions more widely adopted under an industrial mass production setting. Our results demonstrate that stark differences in product selectivity are observed as mass transport is modified. But importantly, they also highlight the promise of TEMPO-catalyzed GOR in opening a new valorization pathway with high selectivity toward valuable C3 products such as MA.

2. Experimental Section

2.1. Materials

All chemicals were purchased from commercial sources andused as received. Na_2CO_3 (ACS reagent, ≥99.5%), $NaHCO_3$ (ACS reagent, ≥99.7%), $NaNO_3$ (ACS reagent, ≥99.0%), NaOH (ACS reagent, ≥97.0%), H_2SO_4 (ACS reagent, 95.0% - 98.0%), H_2O (HPLC plus grade), TEMPO (free radical, 98%), glycerol (ACS reagent, ≥99.5%), oxalic acid (OA, ≥98.0%), sodium mesoxalate monohydrate (≥98.0%), TA (≥98.0%), GLAD (≥98.0%), GA (≥98.0%), FA (≥98.0%), and HPLC-grade ultrapure water were purchased from Sigma–Aldrich. Ag/AgCl reference electrode, Pt wire counter electrode, and 3 mm diameter glassy carbon working electrode were purchased from CH Instruments, Inc. Carbon felt, Sigracet 39AA, and 39BB carbon papers was purchased from Fuel Cell Store. Pt mesh (99.9%, wire diameter 0.06 mm, thickness 0.12 mm, nominal aperture 0.25 mm, 82 × 82, 65% open area) was purchased from Goodfellow Corporation.

2.2. Study of TEMPO-Catalyzed GOR Through Voltammetry and Bulk Electrolysis

2.2.1. Cyclic Voltammetry

CV measurements were performed using a CHI601E potentiostat (CH Instruments, Inc.) with a standard three-electrode configuration including a 3 mm diameter glassy carbon working electrode (geometric area = 0.07 cm^2), an Ag/AgCl reference electrode (3 M KCl) connected to an agar salt bridge (0.1 M $KClO_4$), and a Pt wire counter electrode. All potentials reported in this article are against Ag/AgCl, and no corrections on the obtained current or potentials have been carried out. TEMPO was dissolved in the following electrolyte solutions to acquire a 2 mM solution: 0.5 M H_2SO_4 aqueous solution (pH = 0); 1 M $NaHCO_3$/Na_2CO_3 aqueous buffer solution (pH = 9.2, 10, and 10.6); 0.1 M NaOH and 0.9 M $NaNO_3$ (pH = 13); 1 M NaOH aqueous solution (pH = 14). The three electrodes were placed in a beaker of 10 mL 2 mM TEMPO solution. For each pH, after the initial CV scan in 2 mM TEMPO at 50 mVs^{-1}, glycerol was added to the solution to achieve *c*(glycerol) = 55 mM (40 µL). Then, another CV measurement with the same settings was acquired. The potential window for CV measurements was set to be 0.15–0.85 V versus Ag/AgCl.

2.2.2. Bulk Electrolysis

BE experiments were carried out in a three-compartment W-cell (Adams & Chittenden Scientific Glass Coop, **Scheme2**A) using a CHI601E potentiostat (CH Instruments, Inc.). A 1 × 1 × 1 cm carbon felt working electrode was placed in the central compartment, and an Ag/AgCl reference electrode (3 M KCl) connected to an agar salt bridge (0.1 M $KClO_4$) was placed in a side compartment, while a Pt mesh counter electrode was placed in the other. The working compartment was filled with 5 mL of 5 mM TEMPO dissolved in the appropriate supporting electrolyte solution for each pH value as described above. The counter and reference compartments were filled with enough supporting electrolyte solution to reach the same liquid level as in the working compartment. A magnetic stir bar was used to stir the working solution during electrolysis. The stir rate was controlled electronically by a magnetic stir plate (C-MAG HS 7 control, IKA-Werke GmbH & CO. KG). 8.87 µL glycerol was added to the working compartment to obtain a 20 mM glycerol concentration before the start of BE. The working electrode was held at a constant potential of 0.8 V (vs. Ag/AgCl).

2.3. Study of TEMPO-Catalyzed GOR in Flow Electrolysis

The recirculating flow electrooxidation of glycerol at the anode, mediated by TEMPO, in parallel with the hydrogen evolution reaction at the cathode, catalyzed by platinum, was performed in a gas diffusion electrode-based dual electrolyte channel flow electrolyzer with an active geometric area of 1 cm^2, as described in our previous work, and schematically shown in Scheme 1B.[37–39] Briefly, the flow channel sizing was 2 cm long × 0.5 cm wide with a depth of 0.15 cm. The interelectrode distance was ≈0.30 cm (twice the depth of the channel).

2.3.1. Preparation of Gas Diffusion Layer Electrodes

At the cathode, platinum-sputtered gas diffusion electrodes were used as an electrocatalyst for the hydrogen evolution reaction to compensate for the electrooxidation of glycerol at the anode. An AJA Orion-8 Magnetron Sputtering System (Materials Research Laboratory, UIUC, USA) with a platinum target operating at 50 W and 3 mTorr was used to deposit a film equivalent to 385 nm of platinum onto a Sigracet 39BB gas diffusion layer. This loading corresponded to 1.0 ± 0.1 mg cm^{-2}, as measured by weighing the cathodes before and after the sputtering process. At the anode, a Sigracet 39AA gas diffusion layer was used without any preparation process.

2.3.2. Recirculating Flow Electroanalysis

Peristaltic pumps (Masterflex L/S, Fisher Scientific) were used to recirculate the effluent from each electrolyte stream at 1 mL min^{-1}. An anion exchange membrane (Fumasep Fumion FAA-3-PK-75) soaked for 24 h in pure electrolyte was used to prevent crossover from cathode to anode and vise versa. The electrolyte used was 0.88 M Na_2CO_3 + 0.22 M $NaHCO_3$ (pH 10.6, referenced as "1 M buffer") or 1.0 M NaOH. For the catholyte, 45 mL of pure electrolyte as noted above was used. For the anolyte, 45 mL of electrolyte + 205 mM glycerol + 20 mM TEMPO was used.

Experiments were conducted by applying a constant cell potential using a potentiostat (Reference 600, Gamry Instruments). Individual electrode potentials were monitored using multimeters connected between the appropriate electrode and an Ag/AgCl reference electrode (3 M, RE-5B BASi) in the flow of the appropriate electrolyte. At 22, 45, 90, and 135 min during each experiment, 2 mL of effluent was withdrawn from the recirculation experiment for further product analysis.

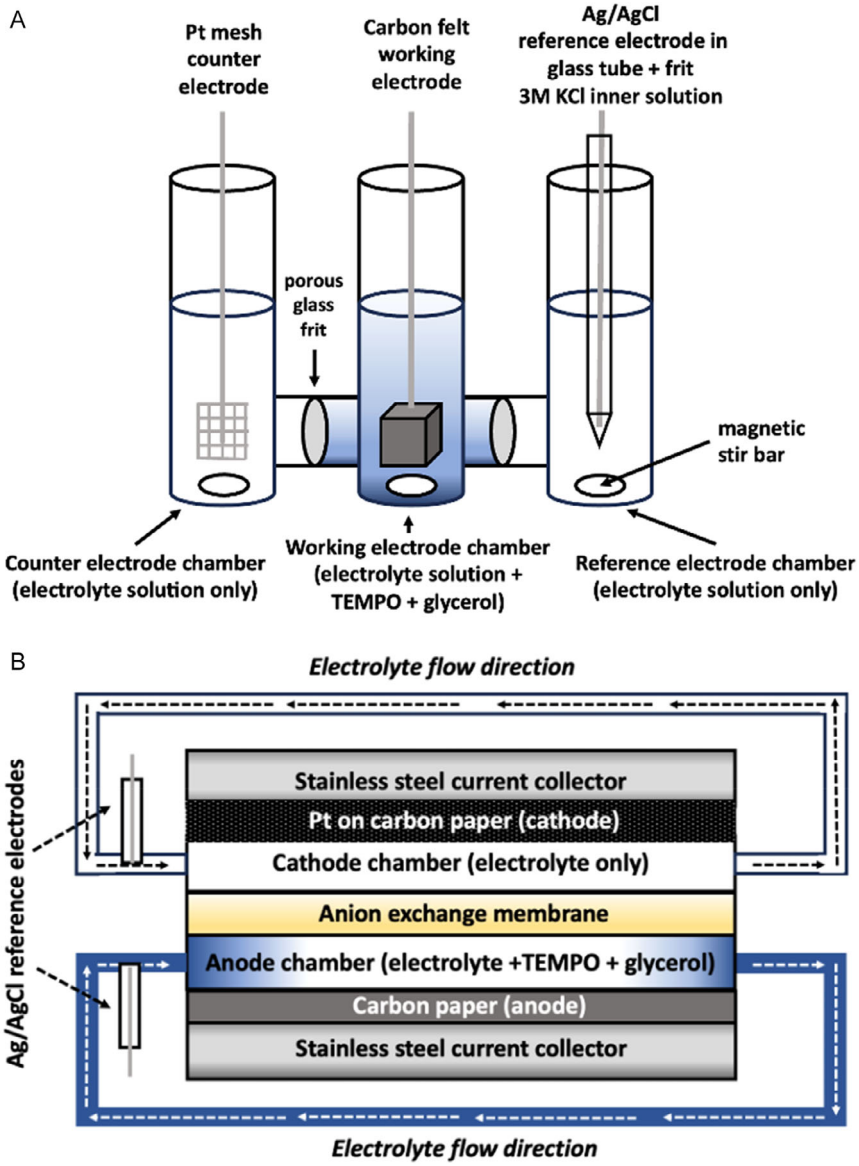

Scheme 2. Experimental electrolysis setups used in this work. A) Stirred bulk electrolysis cell. Depiction of a three-compartment W-cell, where BE experiments were carried out with a carbon felt working electrode (middle compartment), a Pt mesh counter electrode (left compartment), and an Ag/AgCl reference electrode (right compartment). B) Experimental setup of flow electrolysis (FE). Two-compartment flow-by electrolyzer separated by an anion exchange membrane, where FE experiments were carried out with a Pt-sputtered carbon paper cathode (top compartment), a carbon paper anode (bottom compartment), and two Ag/AgCl reference electrodes at the inlet of each stream (left). Electrolyte was recirculated throughout the experiment.

2.4. Product Identification and Quantification with HPLC

HPLC analysis was performed using a Nexera 40 Series HPLC (Shimadzu Scientific Instruments) equipped with a Bio-Rad Aminex HPX-87C column. The samples were prepared by mixing 500 μL of the collected effluent with 500 μL of 5 mM H_2SO_4 made in HPLC-grade ultrapure water. 20 μL of the sample was injected into the column, with temperature control set at 65 °C. The mobile phase was 5 mM H_2SO_4 with a flow rate of 0.6 mL min^{-1}. The separated products were detected with a UV–vis detector (Nexera SPD-40, Shimadzu Scientific Instruments). The concentration of products was determined using the appropriate calibration curves acquired with standards of OA, TA, MA, GLAD, GA, and FA.

3. Results and Discussion

3.1. Effect of pH on the Catalytic Activity and Stability of TEMPO

First, we demonstrate the TEMPO-mediated electrooxidation of glycerol. We conducted CV experiments under different aqueous electrolyte pH of 0, 9.2, 10, 10.6, 13, and 14 while holding other

conditions the same. The ionic strength was kept at 1 M or higher to eliminate any interference on the solution resistance, which affects the current level. For each electrolyte, a CV of 2 mM TEMPO was obtained, followed by another CV measured after the addition of 40 µL glycerol, which resulted in a solution containing 55 mM glycerol and 2 mM TEMPO.

Figure 1 shows that the catalytic activity of electrogenerated TEMPO toward glycerol in solution increases as the pH increases, as indicated by the increasing maximum current level that the CV curves reach as they are scanned toward positive potentials where $TEMPO^+$ is formed. For comparison, the CV for 2 mM TEMPO in the absence of glycerol under the same scan rate conditions is shown in each panel in Figure 1. Except for pH = 0, all panels in Figure 1 show departure from a Nernstian, linearly diffusion-limited CV shape progressively toward a higher current intensity sigmoid shape. This shape is characteristic of mediated electrocatalysis through an EC′ type mechanism where a catalytic chemical step (C′) in the diffusion layer follows a reversible electron transfer step (E) at the electrode.[30,31,40] Although as indicated in Scheme 1B the mediated electrocatalysis process involves a comproportionation step between $TEMPO^+$ and TEMPOH. If this step is fast (e.g., close to diffusion limitation), the system is well described by an EC′ sequence.[30,31] Under otherwise similar conditions, an increase in pH leads to an increase in the measured catalytic current. This effect has been ascribed to OH^- acting as a proton acceptor that helps deprotonate the hydroxyl groups of alcohols, including glycerol, as depicted in Scheme 1B.[26,41,42] The resulting lone pair on the O in the hydroxyl group then reacts with $TEMPO^+$, generating an aldehyde or ketone, with subsequent oxidation of the aldehyde to carboxylic acid.[43–45]

However, we found that pH has an opposite effect on the stability of TEMPO compared to its activity. Figure 1 G–I shows the CV profiles of 5 mM TEMPO solutions before BE and then after running potential-controlled BE (without product separation

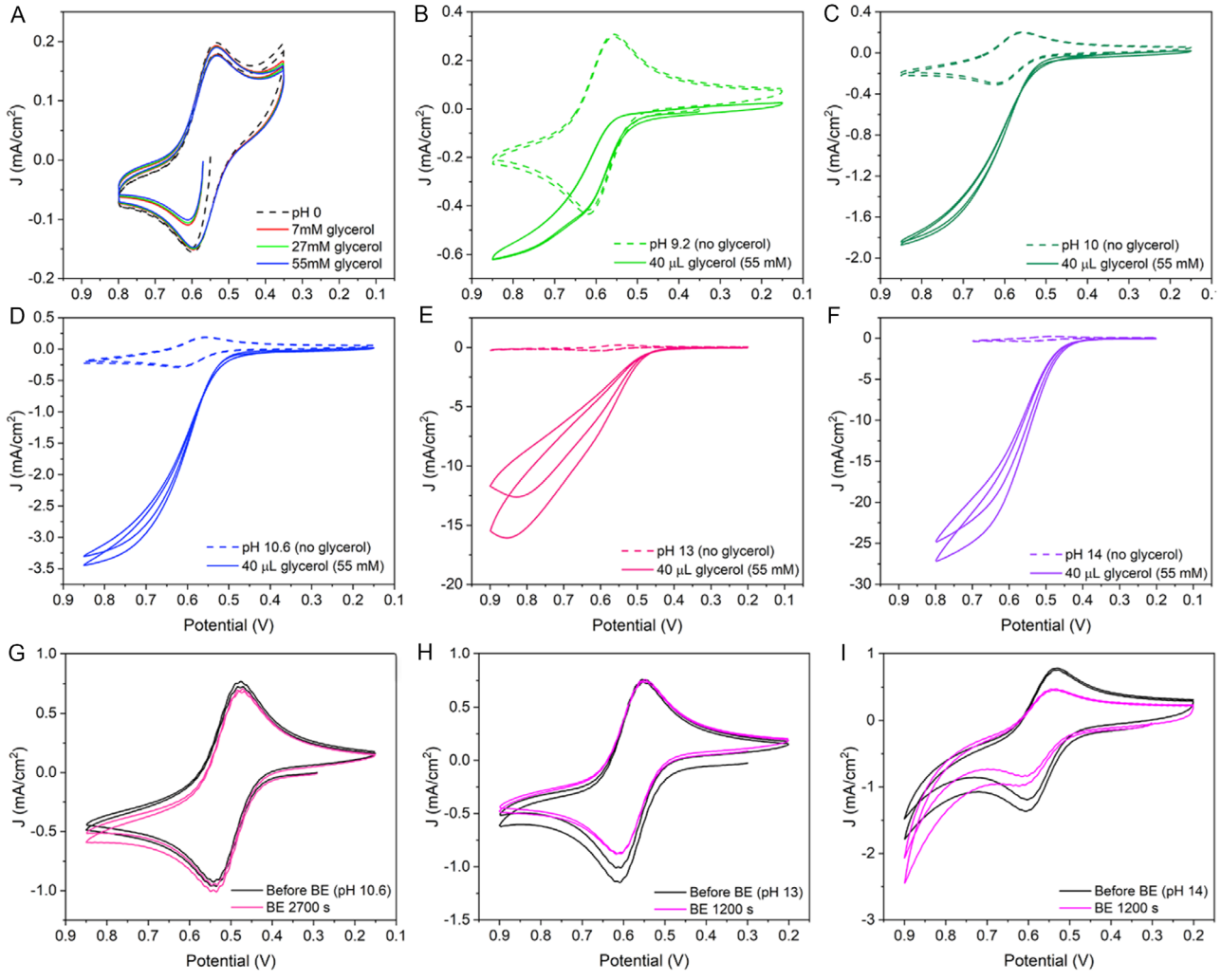

Figure 1. CV measurements of 2 mM TEMPO before (dashed line) and after (solid lines) adding 55 mM glycerol, except for (A), in electrolyte solutions with different pH values. A) pH 0 in 0.5 M H_2SO_4 aqueous solution and adding 7, 27, or 55 mM glycerol; B, C, and D) pH 9.2, 10, and 10.6, respectively, in 1 M $NaHCO_3/Na_2CO_3$ aqueous buffer solution; E) pH 13 in an aqueous solution containing 0.1 M NaOH and 0.9 M $NaNO_3$; F) pH 14 in 1 M NaOH aqueous solution. G–I) CV measurements of 5 mM TEMPO solution before (black) and after (magenta) catalyzing the complete oxidation of 100 µL glycerol (≈137 mM) in electrolytes with different pH values, all acquired at 50 mV s^{-1}. Background electrolyte compositions in (G–I) same as (D–F). The scan rate used in all CV experiments was 50 mV s^{-1}. The area of the electrode was 0.07 cm^2 for all experiments.

steps) at 0.8 V versus Ag/AgCl to oxidize 100 µL glycerol (≈137 mM) for the electrolytes showing the most activity (pH = 10.6, 13, and 14). As the pH increases, a higher portion of TEMPO degrades over the course of catalyzing the complete oxidation of the same amount of glycerol. The degradation is evidenced by a decrease in the peak currents of TEMPO in the CV after BE. At pH 10.6, the CV of TEMPO experiences no significant change before and after the BE process, while at pH 13 and 14, a noticeable drop in the reduction peak current is observed even after shorter BE times required for full electrolysis.

A good catalyst should achieve a higher catalytic reaction rate and great stability simultaneously. However, for TEMPO, there is a trade-off between catalytic activity and stability when varying the solution pH. Therefore, we focused on the 1 M $NaHCO_3/Na_2CO_3$ buffer system (pH = 9.2—10.6) in the following discussion to further investigate the catalyst durability when undergoing three rounds of glycerol oxidation. The carbonate buffer system has been explored before for TEMPO-catalyzed oxidations of alcohols,[32] but to our knowledge, not systematically to explore the performance and stability of TEMPO. For each pH condition (pH = 9.2, 10, and 10.6), three batches of 100 µL glycerol (≈137 mM) were oxidized to completion using 5 mM TEMPO solutions. The glycerol batches were added successively after each BE step and without product or TEMPO separation operations, with CVs taken before and after the reaction of each batch of glycerol. **Figure 2** shows that TEMPO CVs remained relatively unchanged at all three pH values before and after BE and that TEMPO was able to sustain the complete oxidation of three batches of glycerol, totaling 300 µL. This indicates changes within the pH range of 9.2–10.6 do not significantly affect TEMPO stability for the catalysis of GOR. However, due to the difference in the reaction rate, the BE process takes longer at lower pH. The total electrolysis times were 7.90, 3.70, and 2.15 h for pH 9.2, 10, and 10.6, respectively. Therefore, pH 10.6 was decided to be the best condition when considering both catalyst stability and reactivity. Importantly, all BE experiments indicated completion of electrolysis by convergence of the CV to the initial glycerol-free condition. As per the integration of the electrocatalytic current, this occurred when transferring ≈10 equivalents of electrons per molecule of glycerol (n), i.e., $n = 10$. This figure could indicate terminal oxidation to a C3 product such as MA or a partial oxidation resulting in a combination of C1-C3 products. To further elucidate this, we then turned to product analysis.

3.2. Product Analysis in Bulk Electrolysis after GOR

HPLC was used to identify and quantify the products generated by TEMPO-catalyzed GOR in both the batch electrolysis and in flow (vide infra).[4,46] For BE experiments, the yield of different products are shown in **Figure 3**A. Yield is defined as expressed in (Equation 1)

$$Yield(\%) = \frac{n_{product}}{n_{substrate}} \quad (1)$$

where $n_{product}$ is the number of moles of product and $n_{substrate}$ is the initial number of moles of the reaction substrate, in this case, glycerol. The total yield is calculated to be the summation of the yields of all products except for FA, which is accounted for in the balance of OA, since FA and OA are C1 and C2 products, respectively, resulting from C—C scission in glycerol. Theoretically, one glycerol molecule is converted to one FA molecule and one OA molecule. The total yields are over 90% for 1 M $NaHCO_3/Na_2CO_3$ aqueous buffer solution at all pH values, which demonstrates that TEMPO-catalyzed GOR is a promising reaction with very high yields. The main molecule produced during electrolysis is MA, accounting for 60%–80% of the products. MA is a C3 product that precisely corresponds to the 10-electron oxidation of glycerol, consistent with the observations from BE.

To account for the conversion of individual carbon atoms, the metric of carbon balance (CB) is used analogously to previous reports.[23] Here, CB of a certain product is calculated as follows in (Equation 2)

$$CB(\%) = \frac{n_{Cinproduct}}{n_{Cinsubstrate}} \quad (2)$$

where $n_{Cinproduct}$ is the number of moles of C atoms contained in the product and $n_{Cinsubstrate}$ is the total number of C atoms provided by the starting substrate molecules (glycerol, in this case). It is a quantity like yield, but focusing on C atoms instead of individual molecules. When the products are grouped into C1, C2, and C3 products, we can see that C3 products have a CB of

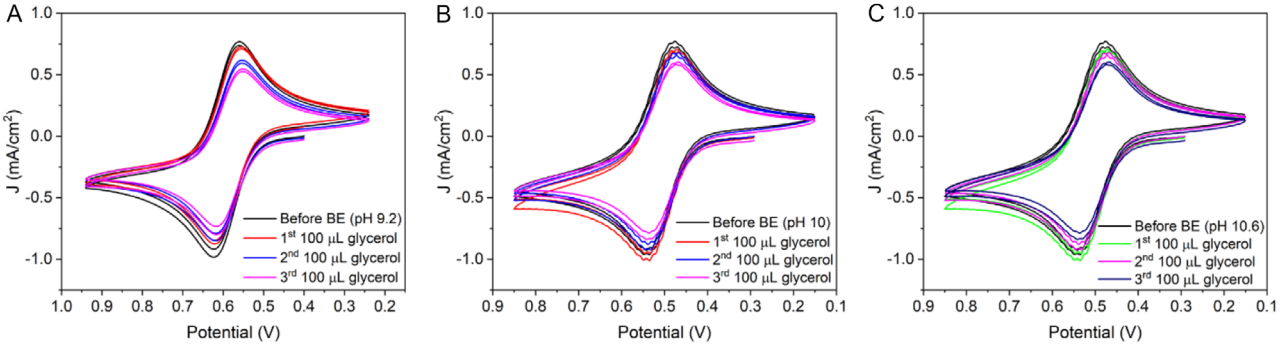

Figure 2. CV measurements of 5 mM TEMPO solution before (black) and after (magenta) catalyzing the complete oxidation of 3 × 100 µL glycerol in electrolytes with pH values of A) pH 9.2, B) pH 10, and C) pH 10.6. All electrolyte solutions are 1 M $NaHCO_3/Na_2CO_3$ aqueous buffer solution. Scan rate of CV is 50 mV s^{-1}, electrode area was 0.07 cm^2.

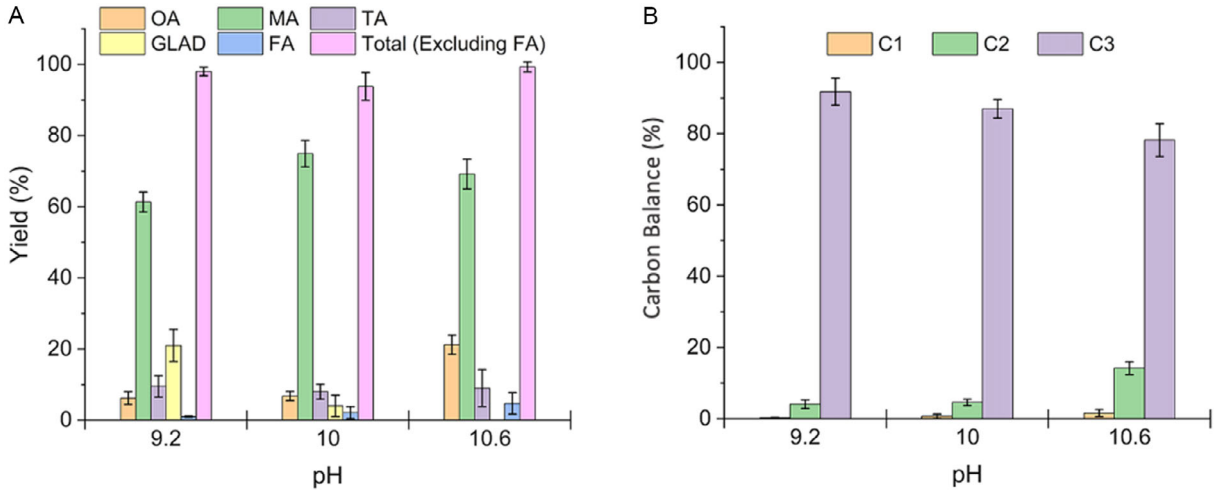

Figure 3. Yields and CB of TEMPO-catalyzed GOR products acquired with BE at different pH. A) Yields of individual products as well as the total yield for each pH. Please note that the total yield (pink bar) is the addition of those for OA, GLAD, MA, and TA. B) CB of C1, C2, and C3 products. Error bars represent the standard deviation of three independent experiments.

78%–92% under all pH values (Figure 3B) with the main product being MA. C3 products are more desirable over C1 and C2 since they are harder to produce and have higher market prices. Thus, TEMPO-catalyzed GOR in a batch process through potential-controlled BE is an attractive pathway toward highly selective C3 molecule production for glycerol valorization.

3.3. Kinetic Characterization of TEMPO-Mediated GOR

To further estimate the rate of the electrochemical process, we carried out electrochemical simulations using the DigiElch 7.0 software. As guided by experiment, we assumed Nernstian heterogeneous kinetics for the TEMPO oxidation at the electrode, mass-transfer limited kinetics for the homogeneous comproportionating reaction of $TEMPO^+$ and TEMPOH, and equal rate constant k_{hom} for any homogeneous reaction involving the two-electron reaction of $TEMPO^+$ with stable intermediate species of glycerol oxidation (denoted S_1, S_2, etc...). The reaction sequence is described in Equations (3)–(6). We acknowledge the simplification of our reaction sequence, where steps 4 and 5 involve proton (H^+) transfer steps in addition to the declared species, as well as coupled hydrolysis reactions; our simulation does not take into account pH (i.e., equilibrium concentrations of H^+ or OH^-).

$$TEMPO^+ + e \rightleftharpoons TEMPO \rightarrow (het., fast) \quad (3)$$

$$TEMPO^+ + glycerol \xrightarrow{k_{hom}} S_1 + TEMPOH \rightarrow (hom.\ 2e\ oxidation\ of\ glycerol) \quad (4)$$

$$TEMPO^+ + S_m \xrightarrow{k_{hom}} S_{m+1} + TEMPOH \rightarrow (hom.\ 2e\ oxidation\ of\ S_m\ until\ m = 4) \quad (5)$$

$$TEMPO^+ + TEMPOH \rightarrow 2TEMPO + H^+ \rightarrow (hom., fast) \quad (6)$$

We used a diffusion coefficient of $0.65 \cdot 10^{-5}$ $cm^2\ s^{-1}$ for all TEMPO-related species,[29] and a diffusion coefficient of $1 \cdot 10^{-5}$ $cm^2\ s^{-1}$ for all glycerol-related species.[47] Following (Equation 5) to the terminal formation of S_5 from S_4, the total number of electrons $n = 10$ represents the formation of MA. This last point was further confirmed by carrying out CV in the presence of TEMPO and sodium mesoxalate (Na_2Meso) at pH 10.6, where **Figure 4**A shows only traces of catalytic activity in comparison to that of glycerol in Figure 1. This establishes that MA is a plausible terminal species, with traces of decomposition to other C1 and C2 products, in agreement with the product distribution observed in Figure 3.

Our simulations, shown in Figure 4B, first confirmed quantitative agreement with the CV of TEMPO in the absence of glycerol, showing only a Nernstian, diffusion limited voltammogram with agreement in peak current and peak position values. Upon addition of glycerol to the experiment and simulation, agreement between the limiting current of the two curves was obtained when k_{hom}, the homogeneous rate constant for oxidation of glycerol and resulting intermediates by $TEMPO^+$, was $\approx 450\ M^{-}\ s^{-1}$. While the simulation targeted matching the limiting current in the sigmoidal voltammogram, there is a good agreement in the overall shape of the experimental and simulated catalytic waves. For a system with little or no substrate depletion during voltammetry (i.e., an EC′ process yielding a sigmoid as observed in Figure 4B) and under conditions where a limiting catalytic current is observed at sufficiently high overpotential (e.g., at a potential of 0.8 V or higher in Figure 4B), the turnover frequency (TOF) of the reaction can be estimated as $TOF = 2{*}k_{hom}{*}C_{substrate}$,[40] where $C_{substrate}$ is the initial concentration of glycerol (0.055 M). Following our analysis of k_{hom} we estimate a TOF of $49.5\ s^{-1}$, which is a high value for TEMPO-based electrooxidations. For comparison, we recently reported on the two-electron TEMPO-mediated oxidation of isopropanol to acetone was $3\ s^{-1}$,[29] and reports for TOFs observed for TEMPO-like catalysts reacting with primary alcohols are also shown to reach a

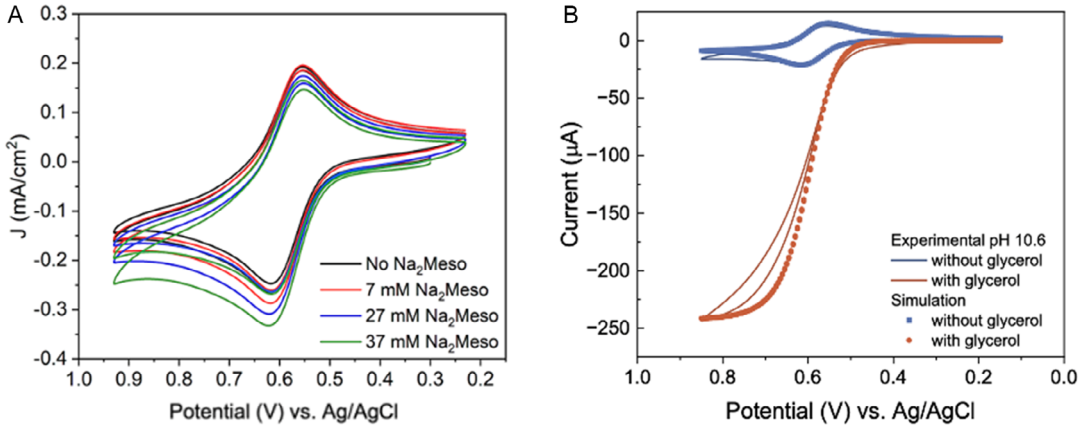

Figure 4. Characterization of terminal oxidation step and electrochemical simulation for TEMPO-catalyzed GOR. A) Electrocatalysis of sodium mesoxalate (Na_2Meso) in pH 10.6 carbonate buffer at the indicated concentrations. B) Comparison of DigiElch simulation and experimental data shown in Figure 1D for 2 mM TEMPO in pH 10.6 in 1 M carbonate buffer with 55 mM glycerol and without glycerol. Please note current is the absolute value and not the current density as in Figure 1D. The area of the electrode was 0.07 cm^2 and all other conditions and parameters as described in the text.

few s^{-1}.[32,48] This high reactivity exhibited in the TEMPO-glycerol system can be exploited in BE to convert larger quantities of glycerol, and also to find optimal conditions for flow electrolysis as described below.

3.4. Rate Optimization of TEMPO-Catalyzed GOR and Flow Electrolysis System

To identify the maximum current density the system can generate with respect to the concentration of TEMPO, *c*(TEMPO), and that of glycerol, *c*(glycerol), a series of CV experiments were conducted varying the concentrations of both compounds. At concentrations lower than *c*(glycerol) = 137 mM, the catalytic oxidative current gradually went up in a 2 mM TEMPO solution as more glycerol was added to the system. When *c*(glycerol) was further increased to 164 mM, the current did not increase further (**Figure 5**A), which indicates the reaction rate is now limited by *c*(TEMPO). Therefore, *c*(TEMPO) was increased to 10 mM, which gave a great improvement in the oxidative current. In this way, *c*(TEMPO) and *c*(glycerol) were iteratively increased until the current reached its maximum under pH 10.6 at *c*(TEMPO) = 20 mM and *c*(glycerol) = 205 mM. Later FE experiments use this condition to reach a high current density. We could not identify conditions exceeding such observed current density, and at concentrations above *c*(TEMPO) = 20 mM we observed the precipitation of an orange oily product, likely indicating its solubility limit under the tested conditions.

We now turn to the comparison of bulk and flow electrolysis. We recognize that setting up an experiment mirroring all components between the two methods is not fully satisfied due to the difference in cell architectures, electrodes (their size, properties, fitting within a cell), and reacting conditions, which place practical constraints. Trying to adapt one experiment to the other may unavoidably miss on optimized performance. For example, potential dependencies that are less relevant for the TEMPO-mediated case here can otherwise lead to dramatic changes in

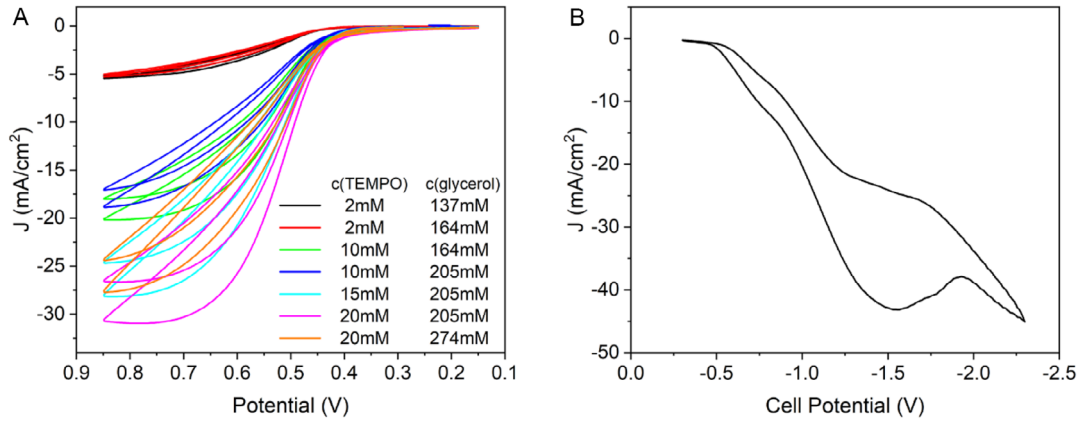

Figure 5. Optimizing current density in the TEMPO-glycerol system. CV measurements in bulk electrolysis cell (nonflow) and flow cell systems in 1 M $NaHCO_3/Na_2CO_3$ aqueous buffer solution at pH 10.6. A) CV measurements to determine the saturating TEMPO and glycerol concentrations to achieve the maximum GOR current. B) CV scan to identify the appropriate cell potential for flow electrolysis in 20 mM TEMPO and 205 mM glycerol. Scan rate of CV is 50 mV s^{-1} in all cases.

product speciation when dealing with heterogenous electrocatalysis.[23] However, given the popularity and broad use of these two techniques, we found it instructive to compare them toward GOR using TEMPO mediation. FE experiments were conducted under the conditions for optimal current density shown in Figure 5A, i.e., *c*(TEMPO) = 20 mM and *c*(glycerol) = 205 mM. A voltametric measurement was obtained while flowing solution at the beginning of the experiment to identify the appropriate cell potential for electrolysis (Figure 5B). Note that the FE system is a two-electrode system and the *x*-axis in Figure 5B is the cell potential. The cell potential was set at −1.5 V, where the GOR current reached its maximum, and where similar current densities to those characterized in the analytical three-electrode CV experiment were observed. Note that the increase in current density beyond −2.0 V is due to processes beyond TEMPO oxidation.

Figure 6A shows the electrolysis current density versus time curve for four different pH values, 9.2, 10, 10.6, and 13.2. The effect of pH on FE current density is similar to that observed in the batch BE system—as pH increases, TEMPO-catalyzed GOR happens at a higher rate. At pH 13.2, even though the initial current level is as high as −36.4 mA cm^{-2}, it rapidly drops after ≈16 min of electrolysis, followed by two other drastic dips at ≈33 min and ≈66 min, eventually reaching a completely failed electrocatalytic reaction with near zero current density. This observation is consistent with the TEMPO degradation observed in BE experiments. On the other hand, the current level at pH 9.2 is the lowest among all four, with a starting value of −10.2 mA cm^{-2} and a slight decrease to −7.0 mA cm^{-2} at around 75 min. A sustained reaction with a stable current density was observed at pH 10 and 10.6. The flow experiment at pH 10.6 gives an average current density of −24.2 mA cm^{-2}, 1.6 times as much as the value at pH 10 (−15.0 mA cm^{-2}). These values were once more consistent with the analytical results in Figure 5A.

Anode potentials were monitored during the FE processes for the tested pH values (Figure 6B). For pH 10 and 10.6, the anode potentials were stable at around 0.49 and 0.57 V, respectively. However, unlike the batch BE where a constant potential of 0.8 V was used, we could not control electrode potential individually in the flow cell since it is a two-electrode system. The cathode and anode potentials are interdependent. This might contribute to the discrepancy in the product speciation for flow and non-FE as discussed later. At pH 9.2 and 13, the anode potential experienced a drop during the experimental process, which corresponds to the sudden decline in current density observed in Figure 6A.

Product speciation changes drastically when switching from the batch BE to the flow system. **Figure 7** compares the obtained chromatograms for both BE and flow experiments. GOR products include OA, TA, and FA, but there is no MA detected in the solution gathered from the FE experiment, and additionally, there is production of GLAD and GA, which were not observed in the batch BE experiment.

The time dependencies of the observed products are shown in Figures 7B and C. FE seems to generate a significantly larger portion of C1-C2 products, as well as C3 products in lower oxidation states. We attempted several modifications to our FE experiments, including changing the materials on the gaskets, current collectors, and carbon supports. In all cases, we observed similar discrepancies between the flow and batch electrolysis experiments, pointing to some fundamentally different process involving mass transfer.

3.5. Discussion on the Comparison Between Bulk and Flow Electrolysis

We hypothesize that the discrepancy comes from the distinct flow patterns and convection properties of the two systems. Reynolds number (Re) is a dimensionless quantity that helps predict fluid flow patterns.[49] For a solution in a container stirred by an agitator, such as our BE experiments, Re is defined as[50]

$$\mathrm{Re} = \frac{2\pi\rho n D^2}{60\mu} \tag{7}$$

where ρ is the fluid density (g mL^{-1}), μ is the fluid viscosity (mPa·s), *n* is the rotational speed of the agitator (rpm), and *D* is the diameter of the agitator. For the flow cell system, Re is calculated as[51]

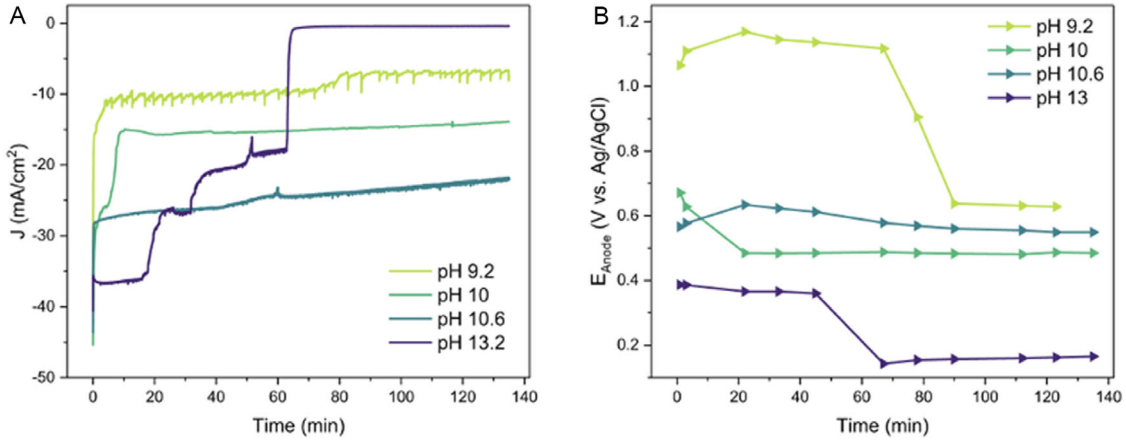

Figure 6. TEMPO-catalyzed GOR at the anode paired to HER at the cathode, performed with a flow cell system with electrolytes at pH 9.2, 10, 10.6 (carbonate buffer systems), and 13.2 (NaOH system). A) GOR current density versus time over the entire course of electrolysis. B) Anode potentials versus time over the electrolysis process. Flow rate is 1 mL min^{-1} for both cathode and anode.

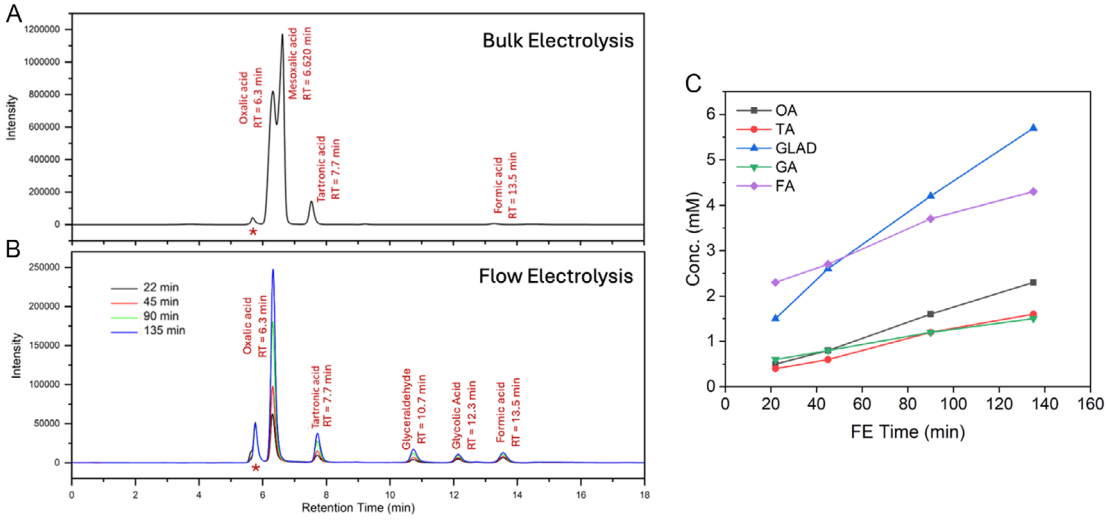

Figure 7. HPLC chromatograms and product distribution for solutions gathered from the BE and flow electrolysis (FE) reaction cell. A) Chromatogram of the reaction solution undergone complete oxidation of glycerol with BE at pH 10.6. B) Chromatograms of the anolyte solution from the flow cell sampled at different stages of the electrolysis at pH 10.6. Notice the absence of mesoxalic acid in (B). Signal intensities in (B) are lower due to lower conversion of the solution. C) Quantification of product distribution in FE from (B) using linear calibration of the chromatographic peaks. The red star in the chromatograms represents a sulfate impurity from the neutralization process used to run HPLC under optimized conditions.

$$\mathrm{Re} = \frac{5}{3}\frac{v\rho l}{\mu h w} \tag{8}$$

where v is the flow rate (mL min^{-1}), and l, h, and w are the length, height, and width of the flow channel (cm), respectively. When the corresponding numbers are inserted into Equations (7) and (8), the Re of the BE and flow cell systems are computed to be 7.5×10^5 ($n = 600$ rpm) and 40 ($v = 1$ mL min^{-1}), respectively. There is a 4 order of magnitude difference in Re for the two setups. The convection is turbulent in the BE cell while laminar in the flow cell, which is possible to make a difference in the reaction pathways and kinetics.

To test the hypothesis that convection can affect the product speciation of TEMPO catalyzed GOR, we performed BE experiments with varying rotational speed and conducted HPLC product analysis on the final reaction solutions (**Figure 8**). The chromatograms show that increasing the stir rate indeed decreases the concentration of OA, a C2 product, which indicates C—C bond cleavage. In other words, high convection helps decrease C—C bond cleavage within glycerol molecules, resulting in a higher selectivity toward C3 products. These experiments suggest that a nonflow, setup such as the stirred, batch BE system used here is more suitable for performing C3-selective TEMPO-catalyzed GOR than the flow cell setup, since high convection can be easily achieved by stirring the solution.

The results above point to stark differences in product selectivity as a function of mass transport mode, creating two opportunities for reflection. First, that considerations on reactor design may not be fully accounted for based on cost or practicality. There is an emerging interest in scaling-up electrocatalytic and electrosynthetic approaches for the industrial production of chemicals,[52] and while considerations of reactor design and their

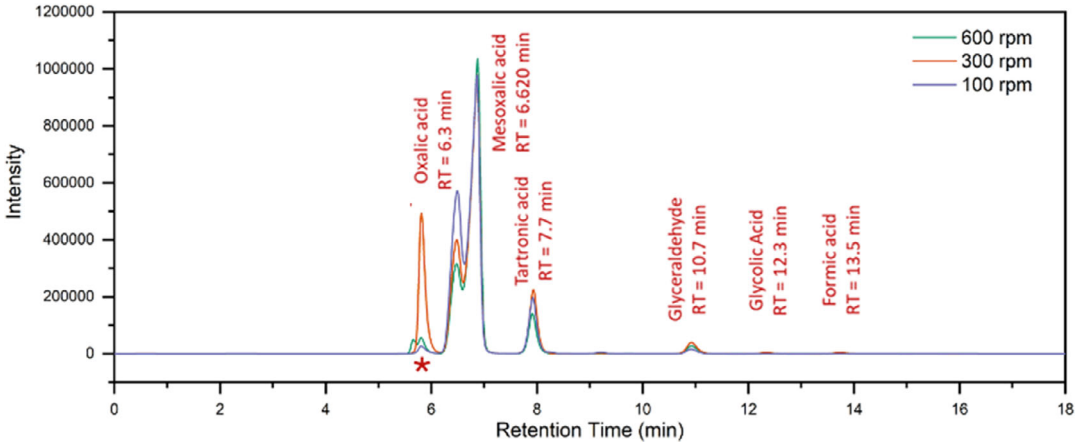

Figure 8. HPLC chromatograms and peak identification for final solutions gathered from the BE experiment at pH 10 with varied stir rate at 600, 300, and 100 rpm. The red star in the chromatograms represents a sulfate impurity from the neutralization process used to run HPLC under optimized conditions.

efficiency are key to economically feasible approaches, they may lead to unmet expectations of product selectivity for certain reactions. Thus, making a connection between the electroanalytical approaches used to explore chemical reactions and their scaling-up is also crucial. The second aspect refers to decoupling the impacts of mass transport and of electrochemical kinetics on product selectivity, an aspect that has also received recent attention in contexts beyond the GOR.[53,54] In this case, developing operando analytical approaches that probe product and intermediate speciation on the electrode and the diffusion layer for each type of reactor design will be key in testing hypotheses on the interplay between dimensionless quantities[52] (e.g., Reynolds number in this study) and chemical species. For example, analyzing the role of interfacial pH during operation,[55,56] the fate of intermediates as they have varying residence times (e.g., hydrolyzable aldehydes in the GOR),[57] or the impact of the relative concentration of reactants within the reaction layer[58,59] would help to better understand phenomena like those reported here.

4. Conclusion

We demonstrated TEMPO as a homogeneous molecular catalyst for glycerol valorization via the GOR with a high current density and selectivity toward valuable C3 products. The dependency of TEMPO catalytic activity and stability on pH was investigated with CV and bulk electrolysis (BE) experiments. As pH increases, TEMPO catalyzes the oxidation of glycerol at a higher rate, but it degrades, compromising its use as a sustainable process. A pH of 10.6 in 1 M carbonate buffer optimized both rate and stability of the reaction, with BE indicating a 10-electron oxidation. CV simulations estimated that the oxidation of glycerol and intermediates by $TEMPO^+$ proceeded with an average homogeneous rate constant of ≈450 $M^{-1}s^{-1}$, resulting in a high TOF of ≈49.5 s^{-1}. Product analysis and targeted CV experiments showed that the main product in the nonflow BE setup was mesoxalic acid (MA), a C3 product. The homogeneous catalysis system was transferred to a flow electrolysis setup with the hope of meeting the requirements of industrial mass-production. A GOR current density of −24.2 mA cm^{-2} was achieved in 20 mM TEMPO and 205 mM glycerol at pH 10.6 with minimal current degradation over 135 min. However, the products generated by TEMPO-catalyzed GOR in the flow cell system exhibited a tendency to produce C1 and C2 products, and no MA. This presents a stirred BE electrolysis setup as a more attractive option for the production of highly valorized C3 products of TEMPO-catalyzed GOR. C3 products, such as MA, TA, and GLAD, are much more valuable (≈$1400, ≈$467, and ≈l$1.85 kg^{-1}, respectively) than C1 and C2 products (FA $0.65 and OA $1.40 kg^{-1}). While a full technoeconomic analysis, including aspects of catalyst loading, separation costs, and energy consumption, is required to make assessments of the most economically viable option, our results highlight the stark difference that glycerol valorization can exhibit between two different electrolysis configurations. This creates new opportunities to re-evaluate the use of mediated electrochemical approaches and batch BE for attaining high-value C3 products from readily available industrial glycerol waste streams.

Acknowledgements

This material is based upon the work supported by the National Science Foundation under the EFRI DCheM program Grant No. 2029326. The authors wish to acknowledge Kristin Martin and Armando Santiago-Carboney for their help with the graphical design of figures and Seth T. Putnam for help with chemical characterization during the revision stage.

Conflict of Interest

The authors declare no conflict of interest.

Author Contributions

Yuanya Zhao: conceptualization (supporting); formal analysis (lead); investigation (lead); methodology (lead); writing—original draft (lead); writing—review & editing (supporting). **Rachel N. Gaines**: conceptualization (supporting); formal analysis (equal); investigation (equal); methodology (equal); writing—original draft (supporting); writing—review & editing (supporting). **Adolfo I. B. Romo**: formal analysis (supporting); methodology (equal); writing—review & editing (supporting). **Juan A. Rojas**: investigation (supporting); writing—review & editing (supporting). **Paul J. A. Kenis**: conceptualization (supporting); funding acquisition (equal); project administration (equal); supervision (equal); writing—review & editing (supporting). **Joaquín Rodríguez-López**: conceptualization (lead); formal analysis (equal); funding acquisition (lead); project administration (lead); supervision (lead); writing—review & editing (lead).

Data Availability Statement

The data that support the findings of this study are available from the corresponding author upon reasonable request.

Keywords: electrocatalysis · electrolysis · glycerol · mesoxalic acid · 2,2,6,6-tetramethyl-1-piperidine-N-oxyl

[1] R. El-Araby, *Biotechnol. Biofuels Bioprod.* **2024**, *17*, 129.
[2] R. Xia, S. Overa, F. Jiao, *JACS Au.* **2022**, *2*, 1054.
[3] S. S. Yazdani, R. Gonzalez, *Curr. Opin. Biotechnol.* **2007**, *18*, 213.
[4] Y. Zhou, Y. Shen, X. Luo, *J. Catal.* **2020**, *381*, 130.
[5] H. W. Tan, A. R. Abdul Aziz, M. K. Aroua, *Renew. Sustain. Energy Rev.* **2013**, *27*, 118.
[6] G. Dodekatos, S. Schünemann, H. Tüysüz, *ACS Catal.* **2018**, *8*, 6301.
[7] J. M. Silva, M. A. Soria, L. M. Madeira, *Renew. Sustain. Energy Rev.* **2015**, *42*, 1187.
[8] C. A. Schwengber, H. J. Alves, R. A. Schaffner, F. A. da Silva, R. Sequinel, V. R. Bach, R. J. Ferracin, *Renew. Sustain. Energy Rev.* **2016**, *58*, 259.
[9] M. Anitha, S. K. Kamarudin, N. T. Kofli, *Chem. Eng. J.* **2016**, *295*, 119.

[10] Q. M. Viana, M. B. Viana, E. A. F. Vasconcelos, S. T. Santaella, R. C. Leitão, *Biotechnol. Lett.* **2014**, *36*, 1381.
[11] Q. He, J. McNutt, J. Yang, *Renew. Sustain. Energy Rev.* **2017**, *71*, 63.
[12] S. Lee, H. J. Kim, E. J. Lim, Y. Kim, Y. Noh, G. W. Huber, W. B. Kim, *Green Chem.* **2016**, *18*, 2877.
[13] D. Sun, Y. Yamada, S. Sato, W. Ueda, *Appl. Catal. B: Environ.* **2016**, *193*, 75.
[14] M. Pagliaro, M. Rossi, *The Future of Glycerol: New Uses of a Versatile Raw Material*, The Royal Society of Chemistry, Cambridge, United Kingdom. **2008**, P014–P015.
[15] A. Hejna, P. Kosmela, K. Formela, Ł. Piszczyk, J. T. Haponiuk, *Renew. Sustain. Energy Rev.* **2016**, *66*, 449.
[16] D. Sun, Y. Yamada, S. Sato, W. Ueda, *Green Chem.* **2017**, *19*, 3186.
[17] B. Katryniok, S. Paul, F. Dumeignil, *ACS Catal.* **2013**, *3*, 1819.
[18] Y. Zhou, Y. Shen, *Electrochem. Commun.* **2018**, *90*, 106.
[19] S. Carrettin, P. McMorn, P. Johnston, K. Griffin, G. J. Hutchings, *Chem. Commun.* **2002**, 696. https://pubs.rsc.org/en/content/articlelanding/2002/cc/b201112n.
[20] S. Bagheri, N. M. Julkapli, W. A. Yehye, *Renew. Sustain. Energy Rev.* **2015**, *41*, 113.
[21] L. Huang, J.-Y. Sun, S.-H. Cao, M. Zhan, Z.-R. Ni, H.-J. Sun, Z. Chen, Z.-Y. Zhou, E. G. Sorte, Y. J. Tong, S.-G. Sun, *ACS Catal.* **2016**, *6*, 7686.
[22] Y. Kim, H. W. Kim, S. Lee, J. Han, D. Lee, J. R. Kim, T. W. Kim, C. U. Kim, S. Y. Jeong, H. J. Chae, B. S. Kim, H. Chang, W. B. Kim, S. M. Choi, H. J. Kim, *ChemCatChem* **2017**, *9*, 1683.
[23] Z. Zhang, L. Xin, L. Qi, D. J. Chadderdon, K. Sun, K. M. Warsko, W. Li, *Appl. Catal. B: Environ.* **2014**, *147*, 871.
[24] A. C. Garcia, M. J. Kolb, N. van, C. Sanchez, J. Vos, Y. Y. Birdja, Y. Kwon, G. Tremiliosi-Filho, M. T. M. Koper, *ACS Catal.* **2016**, *6*, 4491.
[25] C. Dai, L. Sun, H. Liao, B. Khezri, R. D. Webster, A. C. Fisher, Z. J. Xu, *J. Catal.* **2017**, *356*, 14.
[26] R. Gaddam, Z. Wang, Y. Li, L. C. Harris, M. A. Pence, E. R. Guerrero, P. J. A. Kenis, A. A. Gewirth, J. Rodríguez-López, *ACS Catal.* **2024**, *15*, 639.
[27] L. C. Harris, R. N. Gaines, Q. Hua, G. S. Lindsay, J. J. Griebler, P. J. A. Kenis, A. A. Gewirth, *Phys. Chem. Chem. Phys.* **2025**, *27*, 9855.
[28] J. E. Nutting, M. Rafiee, S. S. Stahl, *Chem. Rev.* **2018**, *118*, 4834.
[29] A. Mishra, J. Kim, M. Zorigt, A. I. B. Romo, R. Gaddam, J. E. Braun, D. Ziviani, J. Rodríguez-López, *ACS Sustain. Chem. Eng.* **2023**, *11*, 6241.
[30] M. A. Pence, G. Hazen, J. Rodríguez-López, *Digit. Discovery* **2024**, *3*, 1812.
[31] M. A. Pence, G. Hazen, J. Rodríguez-López, *Anal. Chem.* **2025**, *97*, 6771.
[32] M. Rafiee, K. C. Miles, S. S. Stahl, *J. Am. Chem. Soc.* **2015**, *137*, 14751.
[33] D. P. Hickey, D. A. Schiedler, I. Matanovic, P. V. Doan, P. Atanassov, S. D. Minteer, M. S. Sigman, *J. Am. Chem. Soc.* **2015**, *137*, 16179.
[34] D. P. Hickey, R. D. Milton, D. Chen, M. S. Sigman, S. D. Minteer, *ACS Catal.* **2015**, *5*, 5519.
[35] D. P. Hickey, M. S. McCammant, F. Giroud, M. S. Sigman, S. D. Minteer, *J. Am. Chem. Soc.* **2014**, *136*, 15917.
[36] R. Ciriminna, M. Pagliaro, *Adv. Synth. Catal.* **2003**, *345*, 383.
[37] D. T. Whipple, E. C. Finke, P. J. A. Kenis, *Electrochem. Solid-State Lett.* **2010**, *13*, B109.
[38] S. Ma, M. Sadakiyo, R. Luo, M. Heima, M. Yamauchi, P. J. A. Kenis, *J. Power Sources* **2016**, *301*, 219.
[39] S. Verma, S. Lu, P. J. A. Kenis, *Nat. Energy* **2019**, *4*, 466.
[40] C. Costentin, S. Drouet, M. Robert, J.-M. Savéant, *J. Am. Chem. Soc.* **2012**, *134*, 11235.
[41] Y. Kwon, S. C. S. Lai, P. Rodriguez, M. T. M. Koper, *J. Am. Chem. Soc.* **2011**, *133*, 6914.
[42] Y. Zhang, J.-G. Wang, X. Yu, D. R. Baer, Y. Zhao, L. Mao, F. Wang, Z. Zhu, *ACS Energy Lett.* **2018**, *4*, 215.
[43] R. Ciriminna, M. Ghahremani, B. Karimi, M. Pagliaro, *ChemistryOpen* **2017**, *6*, 5.
[44] A. E. J. d Nooy, A. C. Besemer, H. v Bekkum, *Synthesis* **1996**, *1996*, 1153.
[45] M. Rafiee, B. Karimi, S. Alizadeh*ChemElectroChem* **2013**, *1*, 455.
[46] Y. Zhou, Y. Shen, J. Piao, *ChemElectroChem* **2018**, *5*, 1636.
[47] G. D'Errico, O. Ortona, F. Capuano, V. Vitagliano, *J. Chem. Eng. Data* **2004**, *49*, 1665,
[48] A. Das, S. S. Stahl, *Angew. Chem. Int. Ed.* **2017**, *56*, 8892.
[49] R. B. Bird, W. E. Stewart, E. N. Lightfoot, *Transport Phenomena*, Wiley, United Kingdom **2006**.
[50] R. Raju, S. Balachandar, D. F. Hill, R. J. Adrian, *Chem. Eng. Sci.* **2005**, *60*, 3185.
[51] I. Tosun, D. Uner, C. Ozgen, *Ind. Eng. Chem. Res.* **2002**, *27*, 1955,
[52] M. Regnier, C. Vega, D. I. Ioannou, T. Noël, *Chem. Soc. Rev.* **2024**, *53*, 10741.
[53] J. Jang, M. Rüscher, M. Winzely, C. G. Morales-Guio, *AIChE J.* **2022**, *68*, e17605.
[54] N. B. Watkins, Z. J. Schiffer, Y. Lai, C. B. Musgrave III, H. A. Atwater, W. A. Goddard III, T. Agapie, J. C. Peters, J. M. Gregoire, *ACS Energy Lett.* **2023**, *8*, 2185.
[55] D. A. Henckel, M. J. Counihan, H. E. Holmes, X. Chen, U. O. Nwabara, S. Verma, J. Rodríguez-López, P. J. A. Kenis, A. A. Gewirth, *ACS Catal.* **2021**, *11*, 255.
[56] R. A. Marquez, J. T. Bender, S. C. da Cunha, A. M. Aleman, A. Sahu, V. Ganesan, D. J. Milliron, J. Resasco, T. F. Jaramillo, C. B. Mullins, *ACS Energy Lett.* **2025**, *10*, 2075.
[57] M. Rafiee, Z. M. Konz, M. D. Graaf, H. F. Koolman, S. S. Stahl, *ACS Catal.* **2018**, *8*, 6738.
[58] A. S. Danis, M. J. Counihan, K. O. Hatfield, J. Zhang, G. Agarwal, R. S. Assary, J. Rodríguez-López, *Electrochim. Acta* **2023**, *447*, 142123.
[59] M. Seif-Eddine, S. J. Cobb, Y. Dang, K. Abdiaziz, M. A. Bajada, E. Reisner, M. M. Roessler, *Nat. Chem.* **2024**, *16*, 1015.

Manuscript received: August 26, 2025
Revised manuscript received: October 20, 2025
Version of record online: